Transition to turbulence and effect of initial conditions on three-dimensional compressible mixing in planar blast-wave-driven systems[a]

A. R. Miles,[b] B. Blue, M. J. Edwards, J. A. Greenough, J. F. Hansen, and H. F. Robey
Lawrence Livermore National Laboratory, L-021, 7000 East Avenue, P.O. Box 808, Livermore, California 94551

R. P. Drake, C. Kuranz, and D. R. Leibrandt
University of Michigan, 2455 Hayward Street, Ann Arbor, Michigan 48109

Perturbations on an interface driven by a strong blast wave grow in time due to a combination of Rayleigh–Taylor, Richtmyer–Meshkov, and decompression effects. In this paper, results from three-dimensional (3D) numerical simulations of such a system under drive conditions to be attainable on the National Ignition Facility [E. M. Campbell, Laser Part. Beams **9**, 209 (1991)] are presented. Using the multiphysics, adaptive mesh refinement, higher order Godunov Eulerian hydrocode, Raptor [L. H. Howell and J. A. Greenough, J. Comput. Phys. **184**, 53 (2003)], the late nonlinear instability evolution, including transition to turbulence, is considered for various multimode perturbation spectra. The 3D post-transition state differs from the 2D result, but the process of transition proceeds similarly in both 2D and 3D. The turbulent mixing transition results in a reduction in the growth rate of the mixing layer relative to its pretransition value and, in the case of the bubble front, relative to the 2D result. The post-transition spike front velocity is approximately the same in 2D and 3D. Implications for hydrodynamic mixing in core-collapse supernovae are discussed. © *2005 American Institute of Physics.* [DOI: 10.1063/1.1894765]

I. INTRODUCTION

An interface between two fluids becomes hydrodynamically unstable when it transmits a blast-wave down the density gradient. Perturbations grow under the combined influence of the Rayleigh–Taylor[1,2] (RT) and Richtmyer–Meshkov[3,4] (RM) instabilities. In addition, material decompression behind the shock front results in amplitude stretching that represents a significant contribution to the growth at late times.[5] RM dominates at very early times, but its contribution relative to RT quickly becomes insignificant as the shock-deposited vorticity spreads out and decays away.[5,6] In the nonlinear phase, initial perturbations evolve into spikes of denser material growing in the direction of shock propagation and bubbles of less dense material lagging ever further behind the unperturbed interface position. If the interface is driven by a sufficiently strong blast wave, two-dimensional (2D) and/or 3D secondary instabilities will eventually cause nonlinear spikes to interact with one another and break down. Energy and momentum are thereby diverted into the transverse direction and a transition to a turbulent or turbulentlike state occurs.

In a previous paper, we considered the effect of the initial perturbation spectrum on the nonlinear evolution of a 2D blast-wave-driven system, including spike interaction.[6] Based on high-resolution 2D Raptor[7] simulations, we con-

cluded that memory of certain aspects of the initial conditions, such as the rms amplitude, is retained in the mix width at all times. Spike interaction and breakup was found to correspond to an increase in small-scale mixing, a significant reduction in spike velocity, and a loss of initial transverse spectral information. Consequently, we referred to it as a 2D turbulent mixing transition. At late times, the inverse cascade driven by bubble competition and merger was halted due to drive decay, which imposed an effective box size on the system. After transition but before the emergence of the effective box size, we observed a quasi-self-similar regime during which the similarity parameter $\langle \lambda \rangle / h$ decays slowly in time, with a value only weakly dependent on the initial conditions.

In this paper, we extend this study to include 3D calculations of systems that are otherwise identical to the laser-driven targets described in the 2D paper. Our goal is to determine how the deep nonlinear instability evolution differs in the 3D case, where vortex stretching makes transition to full 3D turbulence possible. In particular, we would like to understand how the initial conditions affect the time to transition and the nature of subsequent turbulent flow.

We will show that nonlinearity thresholds for spike interaction and breakup are not significantly changed in 3D, and that the post-transition state is more thoroughly mixed than in the 2D case. More mix gives a lower effective Atwood number that leads to a large reduction in the bubble growth rate relative to the 2D values despite the decreased drag in 3D. Surprisingly, the velocity of the spike front is not significantly changed when going from 2D to 3D. It is how-

---

ever reduced relative to its pretransition value. This is particularly interesting in light of the fact that 2D simulations of blast-wave-driven mixing in core-collapse supernovae consistently underpredict the asymptotic spike velocities by about a factor of 2 (see Ref. 8 and references therein). This problem is not solved by 3D calculations that predict spike velocities the same as in 2D, suggesting a balance between velocity enhancement due to decreased drag and reduction due to increased small-scale mixing.

II. TRANSITION TO TURBULENCE IN RT-INSTABILITY-DRIVEN SYSTEMS

Before continuing on with simulation results, we wish to clarify what we mean by turbulence. This is particularly important for turbulence in multimode RT systems because there are at least four ideas of turbulence that appear in the literature, and they do not all affect the instability growth in the same way.

First of all, RT-unstable systems can exhibit turbulence in the classical fluid mechanical sense. Unfortunately, there is no universal consensus on what classical turbulence is either. We describe it as a disordered state that undergoes random fluctuations in both space and time and is characterized by energy flow from some large driving scale down to dissipative scales via the 3D phenomenon of vortex stretching. When driven by the RT instability, there is a range of driving scales set by the density spectrum or bubble size distribution. When bubble competition and merger are active, the dominant driving scale for the turbulence grows in time.

Transition to classical turbulence typically requires that the Reynolds number be greater than some threshold value.[9] This requirement amounts to sufficient spectral separation between the driving and dissipative scales. Dimotakis observed[10] that many systems exhibit a transition to a state of increased molecular mixing, which he called the turbulent mixing transition, above a critical Re of about 2×10^4. This corresponds to three orders of magnitude separation between the driving and dissipative scales, allowing for an extended inertial range that is decoupled from both. Above the critical Re for the mixing transition, the internal structure of the flow is less Re dependent than before the transition.

In nonstationary flows, there is a time constraint as well.[11–14] Even if the Reynolds number is high enough that an inertial range can, in principle, exist transition cannot take place until the inertial range has had time to develop. A final requirement for transition that is common to both nonstationary and stationary flows is the existence of some seed perturbation that instabilities can act on. The seed requirement is often not focused on because it will naturally be satisfied in virtually every system, whether physical or computational, due if nothing else to thermal or numerical noise.

The turbulent mixing transition often takes place in flows that have already undergone a transition from a laminar, ordered state to a disordered, spectrally complex state.[10] The term "turbulence" is often also applied to any such system that appears random, regardless of whether or not there is a forward energy cascade via vortex stretching down an inertial range. This includes 3D simulations that leave the

physical dissipation range and much of the inertial range unresolved. The resulting computational Re is often greatly reduced relative to the actual Re in the modeled system, even to the point that there is no discernible inertial range and the computational Re is lower than the experimentally observed critical Re. We will refer to such flows as weakly turbulent or turbulentlike, and to the initiating transition as the weak transition.

Two-dimensional turbulence is distinct from its 3D counterpart in that it lacks the vortex stretching and associated forward cascade that are central to 3D turbulence. There is, however, a forward enstrophy cascade and an inverse energy cascade driven by vortex pairing and merger.[15,16] Since 2D simulations are often used to model 3D turbulent systems, it is important in each case to consider whether or not transition in the 2D system proceeds similarly to transition in the analogous fully resolved 3D system. This will likely depend on whether or not the latter is driven by instabilities that are inherently 3D (such as the Widnall vortex ring instability[17]). In such cases, 2D calculations of course cannot be counted on for predicting the transition time.

Finally, we note that the word turbulence is sometimes used to describe the inverse cascade, driven by bubble competition and merger in 3D as well as in 2D, that is characteristic of nonlinear multimode RT evolution. This continual generation of successively larger scales leads to acceleration of the bubble front and explains the conjectured loss of initial conditions and establishment of a self-similar regime.[18–20] Like transition to classical turbulence, transition to the self-similar regime requires time, space, and a seed. The seed spectrum must contain multiple, incommensurate modes that are unstable (i.e., not so small that they are stabilized by viscosity or other mechanisms). Otherwise, scales larger than those present in the initial conditions cannot be generated and the asymptotic state will be characterized by a stable, periodic array of bubbles. The characteristic wavelength of the spectrum will shift towards the low$-\ell$ end of the initial spectrum, but will not pass beyond it. Noise (including numerical) present in the system can of course serve as the required seed, eventually triggering the interaction and breakup of spikes, but the transition will be delayed.[6]

The space requirement for transition to self-similar turbulence is that the system or box size be at least several times larger than the longest-wavelength significant modes present in the initial conditions.[19] There must also be sufficient time for larger scale to be generated. If the space requirement is not met and until the time condition is satisfied, the scale-invariant bubble distribution[21] will not be realized.

In blast-wave-driven systems (or other system with similarly decaying drive), the effective box size can play the same role as the physical box size in limiting the inverse cascade.[6,22] If the drive becomes very small at late times but does not vanish, then thinking in terms of the effective box size amounts to a transformation of the time requirement into the spatial domain.
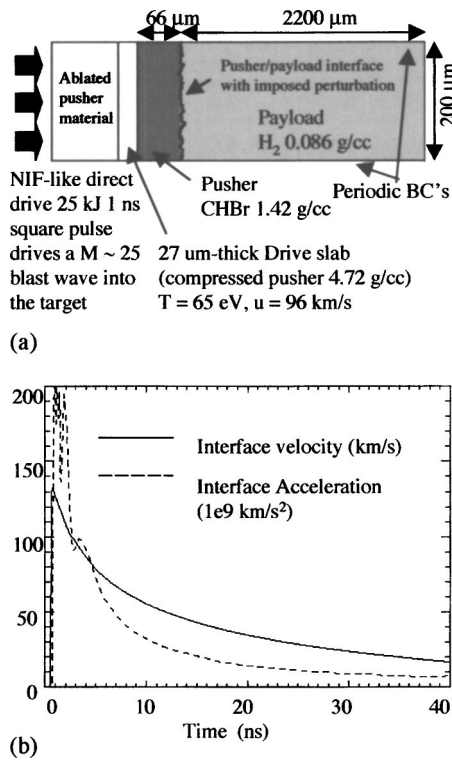
(a)

(b)

FIG. 1. (a) Target schematic (not to scale). (b) Variation in time of interface velocity and deceleration.
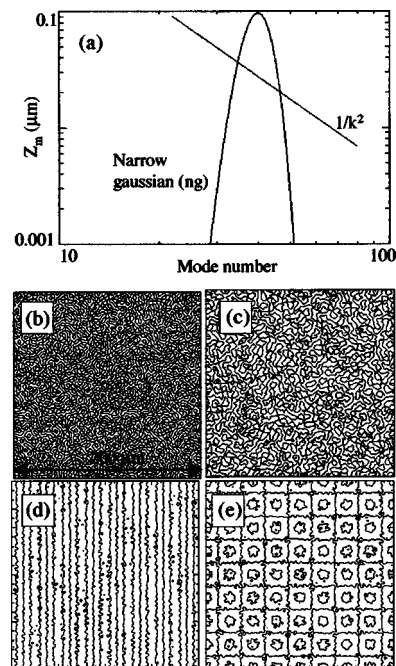

FIG. 2. (a) Initial spectral shapes used for the short-wavelength component in the 3D calculations. Initial interface contour plots: (b) narrow Gaussian (ng), (c) $1/k^2$, (d) narrow Gaussian shorts plus 2D mode 4, and (e) narrow-Gaussian shorts plus mode 4 "egg crate."

III. EFFECT OF TRANSITION ON RT-INSTABILITY GROWTH

The evolution of a RT-unstable interface is likely to be similarly affected by transition to a classically turbulent or turbulentlike 2D or 3D state. Our previous 2D simulations agree with 2D and 3D simulations of others that such transitions leads to a higher degree of small-scale "molecular" mixing and typically a reduction of the growth rate.[6] We have noted, however, that the velocity of the bubble front can be increased if the transition leads to bubble competition in what would otherwise be a stable, periodic array. In that case, transition to a classically turbulent or turbulentlike state provides the seed requirement for a subsequent transition to quasi-self-similar turbulence. In our simulations, the 2D transition was found to occur when the dominant modes in the spectrum reached a nonlinearity threshold of about $h/\lambda \approx 5-6$. For spectrally complex initial conditions, the 2D and self-similar transitions occurred virtually simultaneously. In single or few-mode systems, the self-similar transition sometimes occurred significantly later than the 2D transition.

While transition to a classically turbulent or turbulentlike state leads to enhanced mixing that tends to reduce the RT growth rates,[23,24] transition to a (quasi-)self-similar regime leads to an inverse cascade that tends to enhance the perturbation growth.[25] When both transitions are coincident, the overall effect on the growth rates depends on which effect wins out. Simulations in 2D and 3D tend to show an initial growth rate reduction, especially for the spikes, but the growth must eventually be enhanced if the system allows for unlimited generation of larger structures with higher terminal velocities.[6,24]

We now consider the question of coincidence among the various transitions. It has been proposed that the mixing-transition time in RT-unstable systems is limited by the viscous growth of a shear layer along the spike stalks, and with it the Liepmann–Taylor scale that sets the low$-\ell$ end of the inertial range.[13,14] However, for broadband systems in a big box at high Reynolds number (i.e., seed and space requirements met for both classical and self-similar transitions), the mixing transition is preceded by nearly coincident weak and self-similar transitions. Once modes become nonlinear and begin to couple and generate larger scales, marking transition to self-similar turbulence, spikes soon reach their nonlinearity interaction and breakup thresholds.[6] These interactions drive mix-layer-scale vortices, effectively short circuiting the process whereby the low$-\ell$ end of the inertial range is limited by the viscous growth of a shear layer. Even in 2D, spike interaction and breakup due to Kelvin–Helmholtz (KH) activity results in abrupt growth of small-scale vortices, thereby temporarily mimicking full 3D turbulence characterized by vortex stretching and the associated transfer of energy down to the dissipative scales. Diffusive growth of the shear layer will likely provide the time limitation for transition to classical turbulence only in single-mode or otherwise spectrally simple systems.

When the mixing transition occurs in a system that has already undergone transitions to weak and self-similar turbulence, it can only cause a reduction of the growth rates by effectively lowering the Atwood number within the mix layer.

At low Re, the weak and self-similar transitions need not be coincident. For example, consider that the inverse cascade can occur at any Reynolds number, and in 2D as well as 3D.

Equivalently, the presence of an inverse cascade does not imply strong interactions between spikes and the associated increase in mixedness. The Reynolds number will eventually become high if the inverse cascade is allowed to continue long enough (Re $\sim \lambda^{3/2} g^{1/2}$ if $h \sim \lambda$), but the system can be turbulent in the self-similar sense at lower Re as well.

Conversely, a system with simple modal content can exhibit localized classical turbulence, including the mixing transition, if the Reynolds number is high enough. For example, in RM shock tube experiments by Jacobs and co-workers,[26] secondary instabilities lead to transition to classical turbulence within the KH rollups of single-mode spikes, while the large-scale single-mode structure remains intact and there is no bubble competition. Even so, spike interaction and breakup should increase the extent to which areas of turbulence permeate the mix region.

IV. CALCULATION SETUP AND DESCRIPTION

The simulations are performed using the multiphysics radiation hydrodynamics code Raptor, which uses a second-order (in space and time) Godunov method applied to the Euler equations.[7] Raptor is parallelized and uses adaptive mesh refinement, making it well suited to problems such as ours that require high resolution in only a portion of the computational domain. The calculation setup is nearly identical to our 2D simulations detailed elsewhere,[6] and only an abbreviated description will be given here. The only difference in the 3D calculations is that the initial spectra are now typically 3D, and the nominal resolution is 256 cells across the computational domain instead of 512. The highest level of refinement is reserved for the interface region, and the total number of cells grows with the mix width, eventually reaching over 50×10^6.

Our hypothetical target [see schematic in Fig. 1(a)] consists of a 150 μm plastic pusher section (density 1.42 g/cc) in contact with a cryogenic hydrogen (density 0.086 g/cc) 2.2 mm payload section. An initial perturbation is imposed at the pusher/payload interface, and the width the computational domain was typically 200 μm. Open boundary conditions are used in the parallel (to the shock) direction while periodic conditions are specified in the transverse direction.

The end of the pusher opposite the perturbation is driven with a 25 kJ, 1 ns laser pulse, which launches a strong planar blast wave into the target. Planar experiments with these drive properties will be possible within a few years as the National Ignition Facility[27] becomes operational. The simulations are initiated with a high-velocity, heated, compressed slab with characteristics taken from a laser-driven Lasnex[28] simulation at the end of the laser pulse. Radiation is not included in the Raptor calculations, as the material temperatures are always below 100 eV. The Mach numbers of the incident and transmitted blast waves are in the range of 10–30, where the precise value depends on the degree to which x-ray preheat can be controlled (the incident Mach number with no preheat would be about 60). The resulting initial interface speed is about 130 μm/ns [see Fig. 1(b)]. The post-shock Atwood number remains nearly constant at about 0.7.

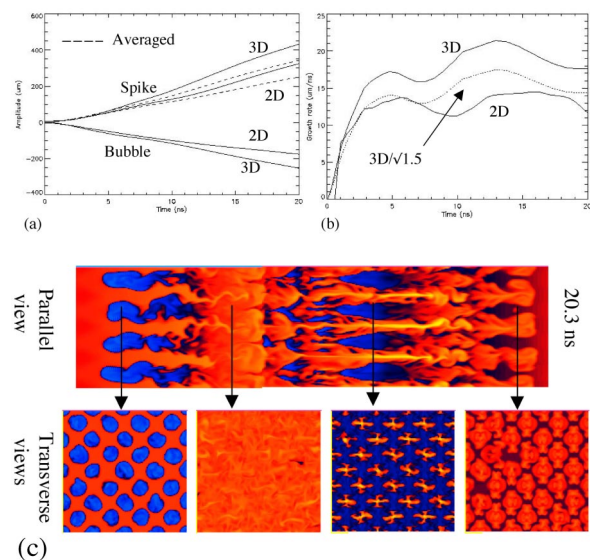In this paper, we will present results from four high-

FIG. 3. (Color online). Effect of dimensionality on single-mode growth (a) amplitudes and (b) averaged growth rate. The 3D growth rate initially saturates at about $\sqrt{1.5}$ (rather than $\sqrt{2.5}$) times the 2D growth rate. (c) Late-time log density image from mode 4 "egg-carton" interface. Despite nonlinearity $a/\lambda = 7$, regular single-scale structure persists along much of the length of the spikes. However, a transition to turbulence appears to have occurred in localized regions where shear layers from individual spikes have merged.

resolution (256 ppb) multimode runs and one low-resolution (128 ppb) mode 4 "egg-crate" run [given by $z_0 = (2.5 \ \mu\text{m})\cos(k_4 x)\cos(k_4 y)$, where k_4 corresponds to the $1 = 4$ mode]. Here and throughout, the number of points per box (ppb) is the number of zones in the transverse direction. Two of the high-resolution multimode runs include only a short wavelength component with modes 20–80 and amplitudes given by a narrow Gaussian in one case and a $1/k^2$ distribution in the other [see Fig. 2(a)]. Each interface was constructed by determining all modes in the annulus satisfying $20 \leqslant (\ell_x^2 + \ell_y^2)^{1/2} \leqslant 80$ (for integer $\ell_{x,y}$) and assigning to each a random phase and randomized amplitude taken from the prescribed distribution. Contour plots of the initial conditions are shown in Figs. 2(b) and 2(c). The other two multimode calculations include a simple long wavelength component in addition to the narrow Gaussian short wavelength component [see Figs. 2(d) and 2(e)]. The long wavelength component is either a single 2D mode 4 or the 3D mode 4 egg crate.

In estimating the Reynolds number in the calculations, we take $\text{Re}_h(t) \equiv [2h(t)/2\Delta x]^{4/3}$ where $2h(t)$ is the mix width and Δx is the cell size. This give a time-dependent Reynolds number that climbs as high as ~ 2200 in the first 18 ns of a 40 ns experiment. This is comparable to the time-independent Reynolds number based on the width of the computational domain $\text{Re}_L = 1626$. If the perturbation amplitude growth is similar in 2D and 3D, then we expect to find $\text{Re}_h \sim 4400$ at 40 ns. The estimated Re number in the actual experiments is of order 10^5, two orders of magnitude greater than in the simulations.[13] Typical of numerical simulations of turbulent systems, the dissipative scales are much smaller than the grid scale. We might expect, however, to qualitatively capture the effect of the turbulence on the large scales
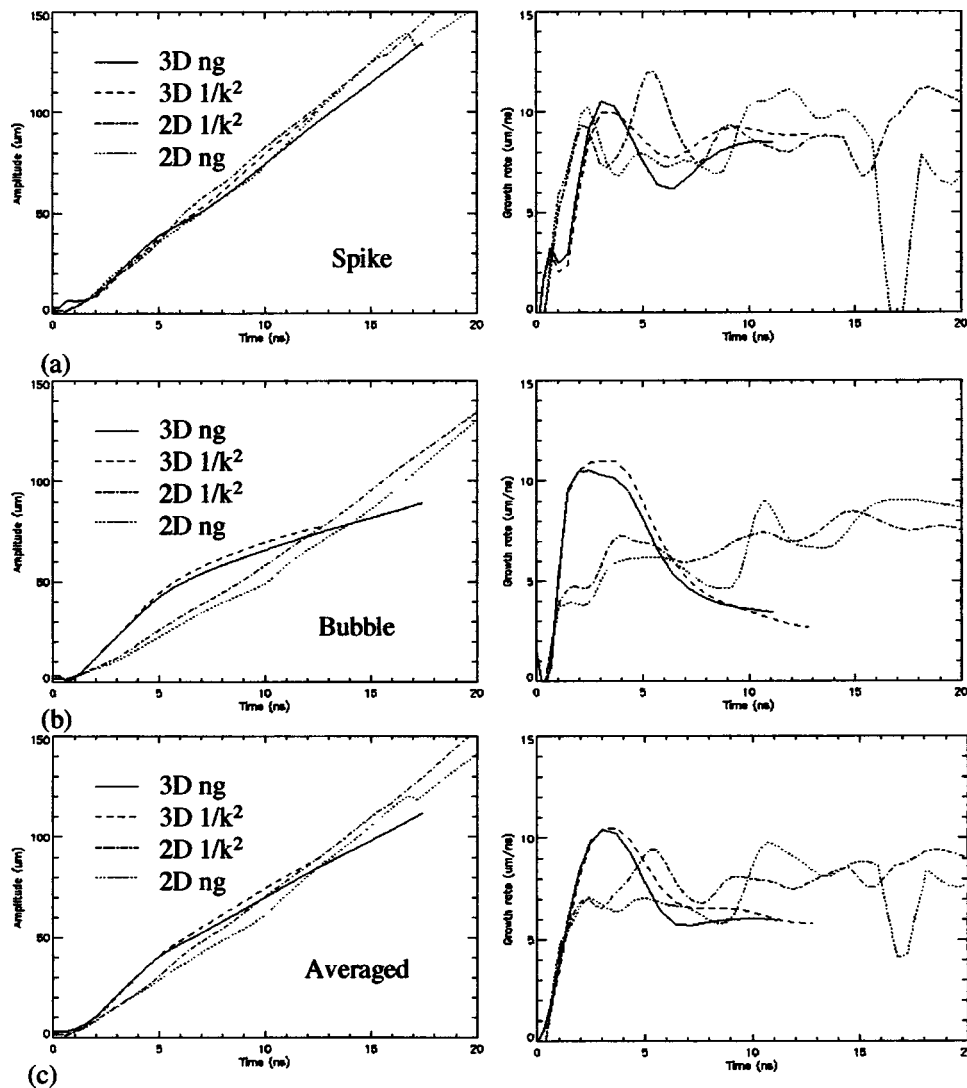
FIG. 4. Perturbation amplitude and velocity histories from narrow Gaussian and $1/k^2$ short wavelength cases. Results from 2D calculations (resolved to 512 ppb) with the same spectral shapes are included for comparison.

if we adequately resolve the lower end of a self-similar inertial range. According to Dimotakis, this scale can be estimated by the Liepmann–Taylor scale, which he defines as $\lambda_{LT}=5L\mathrm{Re}_h^{-1/2}$ where L is the driving scale.[10] With $L=2h$, we find for the experiments $\lambda_{LT}\approx 3-10$ μm. In the simulations, there are then about 4–13 cells per Liepmann–Taylor scale, which corresponds to mode 67–20. Thus we estimate that we are beginning to resolve the upper end of the inertial range with 256 ppb. This estimate is confirmed by spectra presented in Sec. V. We would feel much more comfortable with another factor of 2–4 in resolution, but such calculations are for now prohibitively time consuming.

V. SIMULATION RESULTS

A. Effect of dimensionality on single-mode growth

In Fig. 3, we compare the growth of the mode 4 egg-crate with a single 2D mode 4. The 3D spikes and bubbles have the same transverse scale as the 2D spikes and bubbles, so, during the pretransition phase, the difference in their growth rates should be set by the ratio of their drag coefficients,[25,29,30] $u_{3D}/u_{2D}=\sqrt{C_{2D}/C_{3D}}\approx\sqrt{6\pi/(2\pi\times 1.22)}$ $\approx\sqrt{2.46}\approx 1.57$. In fact, the 3D growth rate initially saturates at about $\sqrt{1.5}\approx 1.2$ times the 2D growth rate [see Fig. 3(b)], possibly because the 3D bubbles appear to develop with a slightly smaller diameter.

A late-time log density image from the mode 4 egg-carton interface is shown in Fig. 3(c). Despite nonlinearity $a/\lambda=7$, regular single-scale structure persists along much of the length of the spikes. However, a transition to turbulence appears to have occurred in localized regions where shear layers from individual spikes have merged. An x-ray radiograph at 25 ns from a 2D short-on-long Omega experiment[31] shows indications of similar localized transitions [see Fig. 9(d)]. Based on the time required for establishment of an inertial range via the viscous growth of the Liepmann–Taylor scale, Robey *et al.* predict that the mixing transition is possible in the experiments after 17 ns.[13] This scenario seems appropriate in this spectrally simple system where there is no weak transition early on.
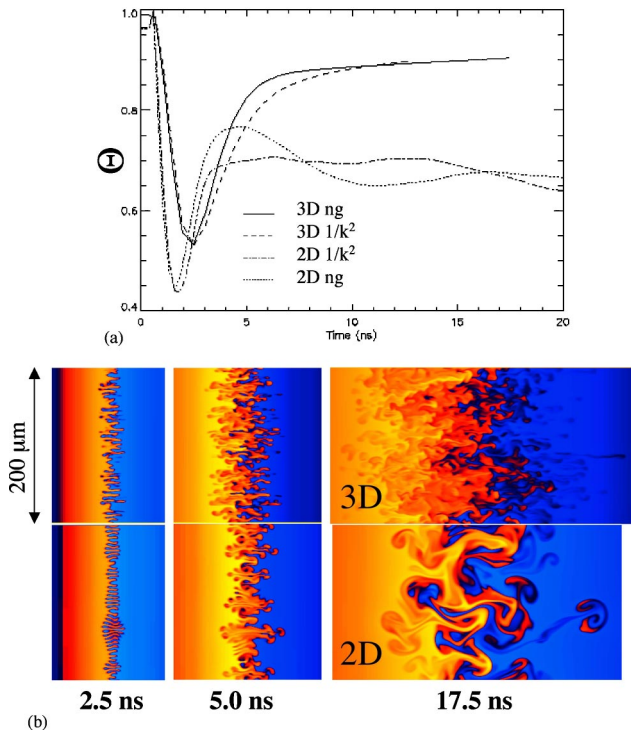
FIG. 5. (Color online). (a) Mixing parameter and (b) log density plots from 2D and 3D ng short-wavelength calculations.

B. Evolution of short wavelength component

Perturbation amplitude and velocity histories from the two high-resolution 3D short wavelength cases are shown in Fig. 4. Results from 2D calculations with the same initial spectral shapes are shown for comparison. In general, the variation between the 3D calculations is slightly less than in 2D. This could be due at least in part to better statistics in the identification of the spike and bubble positions.

At early times, 3D bubbles grow faster than 2D bubbles of the same size. This is expected based on the reduced drag of spherical relative to cylindrical bubbles. At about 5 ns, however, the 3D bubble velocities begin to drop off rapidly, falling to about half the 2D bubble velocity by 10 ns.

Within a few ns after shock transmission, a transition begins from a state with little small-scale mixing to a highly-mixed state [see Fig. 5(a)]. The degree of "mixedness" is determined by using Youngs's "molecular mix," defined by[32]

$$\Theta \equiv \frac{\int \langle f(1-f) \rangle dz}{\int \langle f \rangle dz \int \langle 1-f \rangle dz}, \tag{1}$$

where f and $1-f$ are the volume fractions of the two fluids and the angular brackets denote averaging over the transverse direction. In the 2D calculations, this "2D mixing transition" is complete when the mixing parameter begins to saturate at 4 ns at a level of about 0.7. As we noted previously, this is noticeably higher than the value of about 0.54 obtained by Youngs and Cook *et al.* from their 2D simulations of classical, incompressible RT.[23,24] In 3D, the mixing
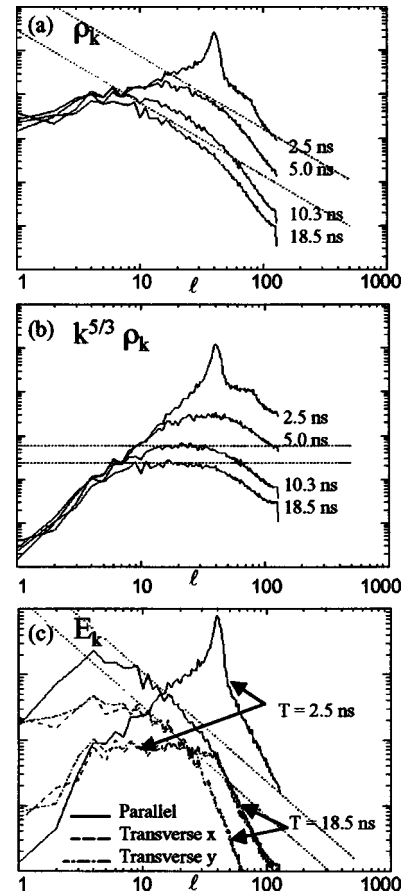

FIG. 6. Time evolution of (a) density spectra ρ_k, (b) $k^{5/3} \rho_k$, and (c) turbulent directed energy spectra. The appearance of an inertial range in the spectra corresponds to the increase in mixedness apparent in Fig. 9(a).

parameter continues to increase until about 10 ns, when it begins to saturate at a higher value of about 0.90. Again, this is higher than the value of about 0.83 reported by Youngs and Cook *et al.*[23,24] Three-dimensional Raptor simulations of classical RT do not show this discrepancy, suggesting that it results from RM, thermal conduction, decompression, or a combination of these effects. We have verified that conduction is not responsible, and do not believe that RM is important after the first few nanoseconds. This leaves decompression, which tends to increase the number of mixed zones at material interfaces. We have not yet determined whether the resulting increase in asymptotic mixedness is a physical or numerical effect.

By about 10 ns, the simulation appears to have undergone a turbulent mixing transition. Indeed, at 90% mixed, it is difficult to imagine what additional mixing transition could possibly take place.

Two-dimensional density and velocity power spectra are integrated over annuli in $k_x - k_y$ space to give a 1D representation that depends only on the magnitude of the transverse wave vector. Results from the 3D narrow-Gaussian case are shown in Fig. 6. The density fluctuation is defined by $\delta\rho(z) = \rho(z) - \langle \rho(z) \rangle$, where $\langle \rho(z) \rangle$ is the z-dependent transverse density average. Each spectrum shown is the average of several (typically four) 1D spectra evenly spaced throughout the interior of the mix region. The inverse cascade to
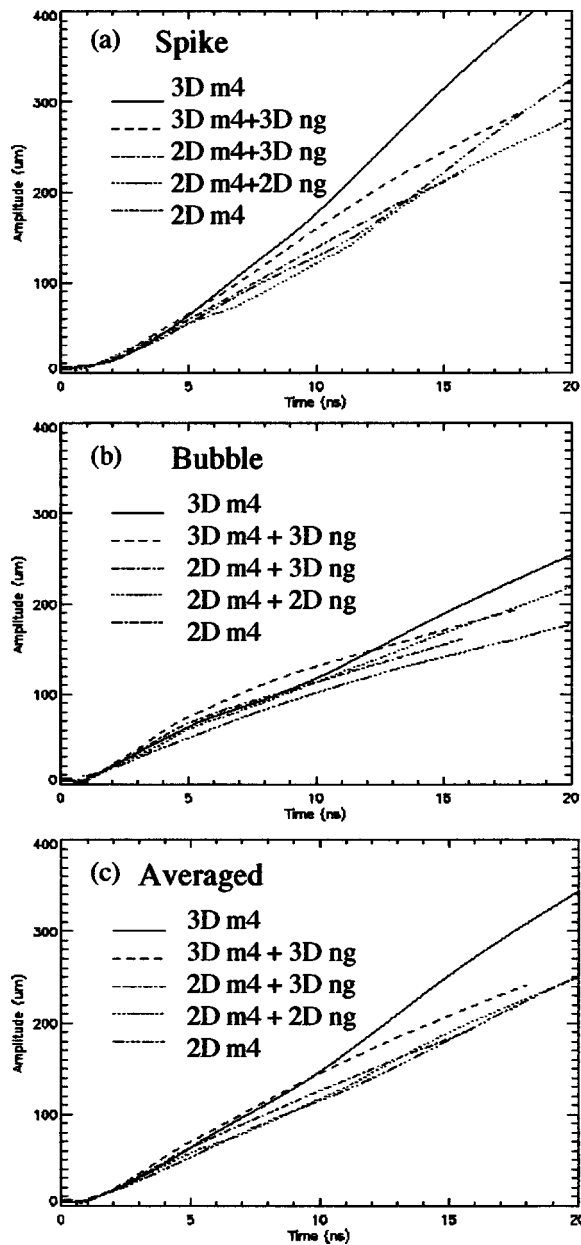
FIG. 7. Perturbation amplitude histories from calculations with mode 4 ($m4$) in the initial conditions. Results from 2D calculations with the same spectral shapes are included for comparison.

FIG. 8. Mixing in simulations with mode 4 ($m4$) in the initial spectra. The 2D calculations show evidence of a weak transition at around 20 ns. The 3D single-mode egg-carton perturbation also shows a transition at around 20 ns, which is the same time that log density plots appear to show localized mixing transitions. When 3D noise is present, the transition happens much earlier (between 10 and 15 ns).

longer wavelengths is apparent in the density spectra. It proceeds rapidly at early times but slows dramatically by 20 ns, indicating the approach of the asymptotic freeze-out stage. This slowing is more apparent in 3D than in our earlier 2D calculations, where vortex pairing and merger contributes to the inverse cascade.

The fluctuating velocity components are defined in the same way as the density fluctuation: $\delta v_{x,y,z}(z)=v_{x,y,z}(z)-\langle v_{x,y,z}(z)\rangle$ where "$\langle\ \rangle$" again denotes transverse average. An inertial range with Kolmogorov $k^{-5/3}$ scaling[33] is visible by about 10 ns in the density spectra from about mode 10 to about mode 30 and in the parallel energy spectra from about mode 10 out to mode 20. The appearance of an inertial range in the transverse energy spectra is somewhat delayed relative to the parallel component. This effect has been previously
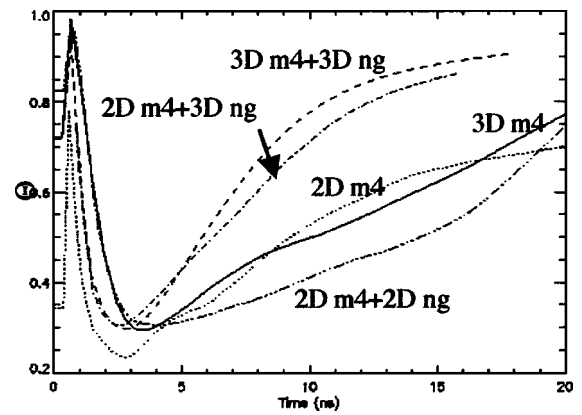
noted in 3D classical RT simulations and attributed to the secondary nature of the transverse flow.[24] That an inertial range appears at all is at first glance surprising considering the relatively limited range of scales present in these simulations and the lack of a sub-grid-scale model. The grid-resolution Reynolds number, defined by $\text{Re}_{\Delta x}\equiv(h/\Delta x)^{4/3}\sim 10^3$, is an order of magnitude smaller than the integral-scale Reynolds number observed by Dimotakis[10] to mark the mixing transition in many flows. It appears, however, that the effective integral-scale Reynolds number is much higher than the grid-resolution Reynolds number. Following the scaling used by Dimotakis, we find that the ratio of the lower end to the upper end of the inertial range is approximately given by $0.1\,\text{Re}^{1/4}$. Based on the inertial range observed in the calculated spectra, this gives $\text{Re}>10^5$. As predicted by Dimotakis, the appearance of the inertial range corresponds with a turbulent mixing transition.

It is important to note that the 3D bubble velocity falls off precisely while the 3D mixedness is increasing above the value seen in the 2D calculations. This suggests that the increased mixing in the bubble region has resulted in a lower effective Atwood number and, consequently, a lower growth rate.

In this spectrally complex system, the time to transition does not seem to be limited by the viscous growth of a shear layer as was suggested in the 3D single-mode calculation. Instead, transition is triggered by strong interactions between neighboring spikes. When the dominant spikes reach their nonlinear breakdown thresholds, a significant fraction of their energy is diverted into the transverse direction, resulting in forcing of mix-layer-scale vortices. Since this happens earlier when the characteristic mode number in the spectrum is higher, the transition here takes place earlier than it does in the single-mode system despite the fact that the integral scale (the mix width) is much smaller.

C. Effect of shorts on long

Two high-resolution, 3D, short on long simulations were run. In each case, the short wavelength component was the same 3D narrow Gaussian shown in Figs. 2(a) and 2(b) and
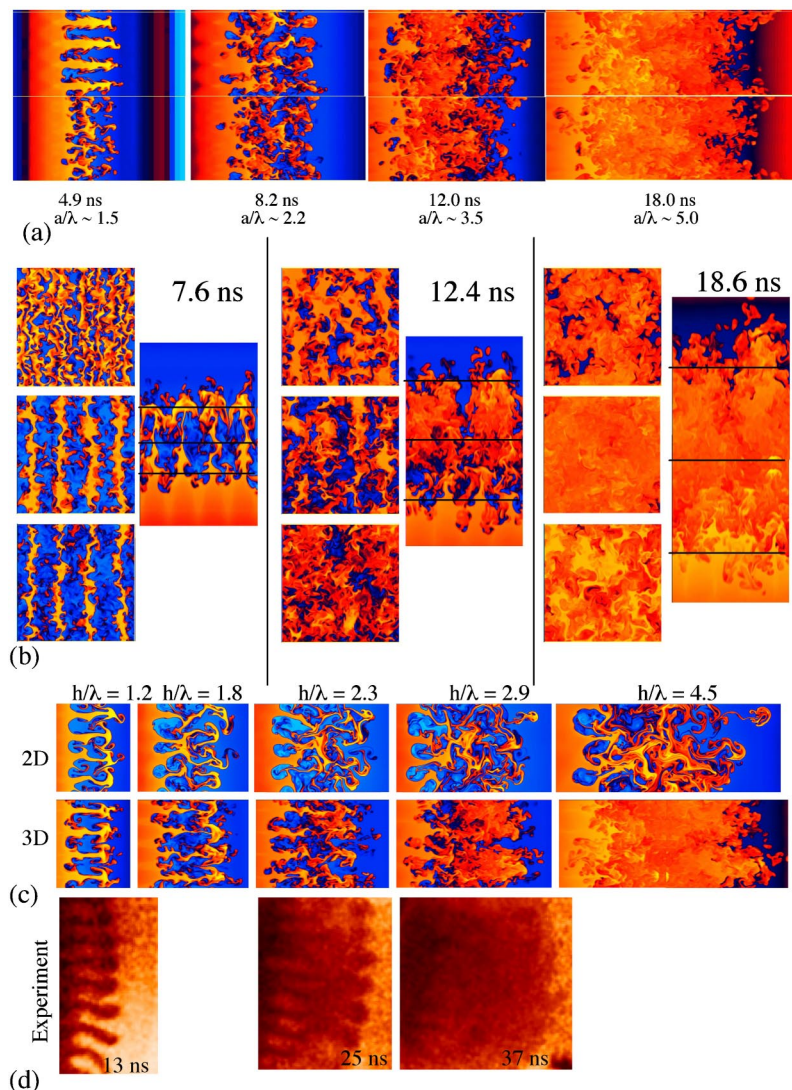
FIG. 9. (Color online). Log density plots of the evolving mix layer from the (a) 3D$m4$+3Dng calculation and (b) 2D$m4$+3Dng calculations. In (a), the upper row of slices is taken from a spike position, and the lower row from a bubble position. In (b), solid lines in parallel slices denote approximate locations of transverse slices. Spike interaction (between the mode 4 spikes) begins when $a/\lambda \approx 2$. A very clear transition to a well-mixed state has taken place by 18 ns, at which point $a/\lambda \approx 5$. In the 2D $m4$ case, the interior of the mix region remains anisotropic in the transverse plane until the mixing transition has taken place. (c) Comparison with the analogous 2D calculation (2D$m4$+2Dng) illustrates the importance of 3D effects. The post-transition state depends strongly on the dimensionality, but the process of transition proceeds similarly in 2D and 3D. (d) X-ray radiography from a 2D short-on-long Omega target shows indications of transition at the same degree of nonlinearity as predicted by the simulations.

used in Fig. 5. The long-wavelength component was a 2D mode 4 (2D$m4$) in one case and a mode 4 "egg carton" (which we will call 3D mode 4 or 3D$m4$) in the other. Amplitude histories from these calculations are shown in Fig. 7 along with results from 2D$m4$, 3D$m4$, and 2D narrow-Gaussian shorts on a 2D mode 4 (2D$m4$+ng). In each case, the amplitude of mode 4 was 2.5 μm ($a/\lambda=0.05$), and the rms amplitude of the short-wavelength component was ten times smaller.

The large reduction in bubble growth seen with the short-wavelength distribution is not so apparent when mode 4 is present [see Fig. 7(b)]. We believe that this is because it takes much longer for mode 4 to grow up to its nonlinear interaction and breakdown thresholds. Consequently, the mixing transition does not occur until between 10 and 15 ns (see Fig. 8). This is consistent with the conclusion we made based on our 2D calculations that the presence of a long-wavelength mode with significant initial amplitude can delay the transition to a turbulentlike state.

Log density slices through the evolving mix layer from the 3D$m4$+3Dng calculation are shown in Fig. 9(a). The dominant mode 4 spikes begin to interact with one another when $a/\lambda \approx 2$, or approximately one eddy turnover time after

the perturbation grows nonlinear and large vortices develop at the spike tips. A very clear transition to a well-mixed state has taken place by 18 ns, at which point $a/\lambda \approx 5$ and 1–2 additional largest-scale eddy turnover times have elapsed. These same nonlinear thresholds for spike interaction and breakdown/transition were found in our 2D calculations.[6] Thus it appears that, for complex initial spectra, transition in blast-wave-driven systems proceeds similarly in 2D and 3D, indicating that three-dimensional secondary instabilities do not play a dominant role in initiating the transition. Again, the mixing transition corresponds to the loss of transverse spectral information and the appearance of an inertial range with $\mathbf{k}^{-5/3}$ scaling [see Figs. 10(a) and 10(b)].

The 2D$m4$+3Dng evolves similarly except that the interior of the mix region remains anisotropic in the transverse plane until the mixing transition has taken place [see Figs. 9(b), 10(c), and 10(d)]. The post-transition mix width remains somewhat smaller than with the egg-carton perturbation, but the two flows are otherwise very difficult to distinguish.

Figure 9(c), which is a side-by-side comparison of 2D$m4$+2Dng and 2D$m4$+3Dng, provides a useful illustration of the importance of 3D effects. Early on, 3D effects are
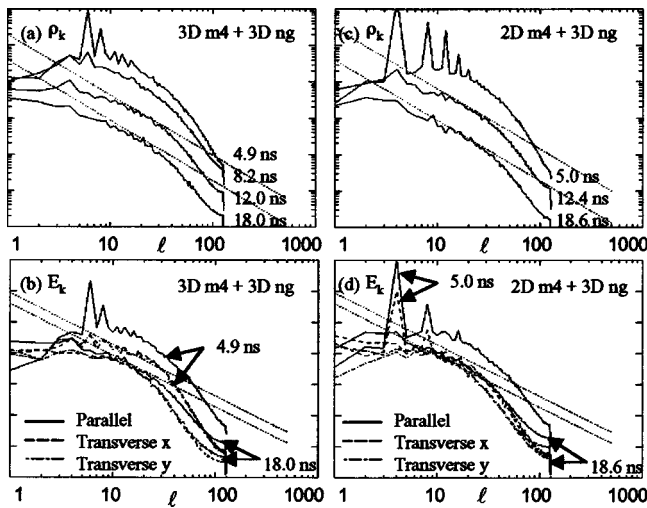
FIG. 10. Density and energy spectra from the 3D*m*4+3D*n*g and 2D*m*4 +3D*n*g calculations. An inertial range is apparent by the time the mixing transition has taken place. Even in the 2D*m*4 case, the transverse velocity spectrum is nearly isotropic after the mixing transition.

not important. In both cases, a transition at about 10 ns takes the interface to a less ordered, more mixed state. The post-transition state is very different in 2D and 3D, but the process of transition is not. Radiography from the 2D short-on-long experiment discussed in Ref. 31 shows evidence of transition when the perturbation reaches the same degree of nonlinearity as in the simulations [see Fig. 9(d)]. The time at which transition occurs is later in the experiment because the Omega drive was five times less energetic than in the NIF system.

VI. CONCLUSIONS

When an RT-unstable interface grows to several times its characteristic wavelength, it can undergo a "weak transition" to a disordered, apparently random state. This transition proceeds similarly in 3D and 2D systems with approximately equal nonlinear spike interaction and breakdown thresholds. In the latter case, it can lead to 2D turbulence with an inverse energy cascade due to vortex pairing and merger. A separate inverse cascade in 3D as well as 2D systems follows transition to the self-similar regime of bubble competition and merger. In systems that are not spectrally simple, the weak and self-similar transitions are likely to occur nearly simultaneously. In 3D systems, a subsequent mixing transition leads to fully-developed classical turbulence if the Reynolds number is high enough. Because the post-transition interface region is more thoroughly mixed in 3D than in 2D, its growth is more suppressed relative to the single-mode case.

Each of these transitions has time, space, and seed requirements that must be met before it can occur. The time requirement for the mixing transition may be given by a viscous diffusion time for spectrally simple systems, but is more likely to be set by a nonlinearity threshold for strong spike interaction and breakdown when the initial conditions are spectrally complex.

The weak, 2D, and mixing transitions lead to increased small-scale mixing that reduces the instability growth rate at

least temporarily. Wherever it occurs, the self-similar transition will eventually give accelerated growth if it is allowed to proceed unhindered by system size or drive time constraints. For interfaces that have already undergone a transition to self-similar growth, a subsequent mixing transition can only inhibit future instability growth.

These conclusions are in large part born out by 2D and 3D Raptor calculations of planar blast-wave-driven systems. The 3D calculations have not yet reached the freeze-out stage, but do appear to exhibit a mixing transition despite a grid-resolution Reynolds number only of order a thousand. Whether or not the current resolution captures enough of the inertial range that further increases in resolution will be unnecessary remains for now an open question.

The simulations show sensitive dependence on the initial conditions deep in the nonlinear post-transition phase of the instability growth. Where the low mode 4 is included in the initial conditions, the late-time mix width is much larger. It could be argued that the boundary conditions are affecting the growth at this stage, but that effect should be to inhibit the growth rather than suppress it. Perhaps if the transverse domain could be made arbitrarily large and the drive sustained arbitrarily long, the shorts only and short-on-long systems would begin to look very similar. However, at 20 ns we are already nearing the freeze-out stage, in which differences in perturbation amplitude will be preserved at later times.

Thus three-dimensional effects do not add anything that will counter the tendency of blast-wave-driven systems to remember some aspects of the initial conditions. For supernova calculations, this means that an understanding of the initial conditions is important for getting that late-time mix width correct. Experiments should include similar initial conditions in order to be truly relevant to supernova. In particular, spectrally simple initial conditions are of limited utility since even the process by which they undergo transition may be different than with more realistic multimode spectra.

ACKNOWLEDGMENT

[1]Lord Rayleigh, *Scientific Papers* (Cambridge University Press, Cambridge, 1899).

[2]G. I. Taylor, Proc. R. Soc. London, Ser. A **201**, 192 (1950).

[3]R. D. Richtmyer, Commun. Pure Appl. Math. **13**, 297 (1960).

[4]E. E. Meshkov, Izv. Akad. Nauk SSSR, Mekh. Zhidk. Gaza **4**, 151 (1969).

[5]A. R. Miles, D. G. Braun, M. J. Edwards *et al.*, Phys. Plasmas **11**, 3631 (2004).

[6]A. R. Miles, M. J. Edwards, and J. A. Greenough, Phys. Plasmas **11**, 5278 (2004).

[7]L. H. Howell and J. A. Greenough, J. Comput. Phys. **184**, 53 (2003).

[8]K. Kifonidis, T. Plewa, H.-Th. Janka, and E. Muller, Astron. Astrophys. **408**, 621 (2003).

[9]H. Tennekes and J. L. Lumley, *A First Course in Turbulence* (MIT, Cambridge, 1972).

[10]P. E. Dimotakis, J. Fluid Mech. **409**, 69 (2000).

[11]G. G. Stokes, Trans. Cambridge Philos. Soc. **9**, 8 (1851).

[12]D. Galmiche and S. Gauthier, Jpn. J. Appl. Phys. **35**, 4516 (1996).

[13]H. F. Robey, Ye Zhou, A. C. Buckingham, P. Keiter, B. A. Remington, and R. P. Drake, Phys. Plasmas **10**, 614 (2003).

[14]Ye Zhou, H. F. Robey, A. C. Buckingham, Phys. Rev. E **67**, 056305 (2003).
[15]R. H. Kraichnan, Phys. Fluids **10**, 1417 (1967).
[16]M. A. Rutgers, Phys. Rev. Lett. **81**, 2244 (1998).
[17]S. E. Widnall, D. B. Bliss, and C. Tsai, J. Fluid Mech. **66**, 35 (1974).
[18]K. I. Read, Physica D **12**, 45 (1984).
[19]D. L. Youngs, Physica D **12**, 32 (1984).
[20]U. Alon, J. Hecht, D. Mukamel, and D. Shvarts, Phys. Rev. Lett. **72**, 2867 (1994).
[21]J. Glimm and D. H. Sharp, Phys. Rev. Lett. **64**, 2137 (1990).
[22]A. R. Miles, Phys. Plasmas **11**, 5140 (2004).
[23]D. L. Youngs, Laser Part. Beams **12**, 725 (1994).
[24]A. W. Cook, W. H. Cabot, and P. L. Miller, J. Fluid Mech. **511**, 333 (2004).

[25]D. Layzer, Astrophys. J. **122**, 1 (1955).
[26]M. A. Jones and J. W. Jacobs, Phys. Fluids **9**, 3078 (1997); B. D. Collins and J. W. Jacobs, J. Fluid Mech. **464**, 113 (2002).
[27]E. M. Campbell, Laser Part. Beams **9**, 209 (1991).
[28]G. B. Zimmerman and W. L. Kruer, Comments Plasma Phys. Controlled Fusion **2**, 51 (1975).
[29]R. M. Davies and G. I. Taylor, Proc. R. Soc. London, Ser. A **200**, 375 (1950).
[30]D. Oron, L. Arazi, D. Kartoon, A. Rikanati, U. Alon, and D. Shvarts, Phys. Plasmas **8**, 2883 (2001).
[31]A. R. Miles, M. J. Edwards, B. Blue *et al.*, Phys. Plasmas **11**, 5507 (2004).
[32]D. L. Youngs, Phys. Fluids A **3**, 1312 (1991).
[33]A. N. Kolmogorov, Dokl. Akad. Nauk SSSR **31**, 538 (1941).